# Soil Moisture Estimation with GNSS Reflectometry: a Conceptual Review

*Estimativa da Umidade do Solo por Refletometria GNSS: uma Revisão Conceitual*

Jorge Felipe Euriques [1], Claudia Pereira Krueger [2], Wagner Carrupt Machado [3], Luiz Fernando Sapucci [4] and Felipe Geremia-Nievinski [5]

1 Universidade Federal do Paraná, Departamento de Geomática, Programa de Pós-Graduação em Ciências Geodésicas, Curitiba, Brasil. jorge.euriques@gmail.com
 ORCID: https://orcid.org/0000-0001-9234-7551
2 Universidade Federal do Paraná, Departamento de Geomática, Programa de Pós-Graduação em Ciências Geodésicas, Curitiba, Brasil. cpkrueger64@gmail.com
 ORCID: https://orcid.org/0000-0002-4839-1317
3 Universidade Federal de Uberlândia, Centro de Ciências Exatas e Tecnologia, Monte Carmelo, Brasil. wagnercarrupt@ufu.br
 ORCID: https://orcid.org/0000-0003-3112-7808
4 Instituto Nacional de Pesquisas Espaciais, Centro de Previsão de Tempo e Estudos Climáticos, Programa de Pós-Graduação em Meteorologia, Cachoeira Paulista, Brasil. luiz.sapucci@inpe.br
 ORCID: https://orcid.org/0000-0001-8420-8033
5 Universidade Federal do Rio Grande do Sul, Departamento de Geodésia, Programa de Pós-Graduação em Sensoriamento Remoto, Porto Alegre, Brasil. felipe.nievinski@ufrgs.br.
 ORCID: https://orcid.org/0000-0002-3325-1987

**Abstract:** Soil moisture monitoring enables efficient management and use of water resources, having great importance for several purposes, such as: monitoring of risk areas; delimitation of areas susceptible to flooding; geotechnical activities; and in agriculture development. GNSS Reflectometry (GNSS-R) is a scientific and technological development that allows one to perform proximal or remote sensing, depending on the antenna height concerning the surface, by means of navigation satellites. This method exploits GNSS signals indirectly reaching a receiver antenna after they are reflected on the surrounding surfaces. In this method, direct and indirect GNSS signals that reach the receiving antenna are exploited, after reflection on the surfaces existing around the antenna. The combination of these two signals causes the multipath effect, which affects GNSS observable and deteriorates positioning. On the other hand, when interacting with these reflecting surfaces one can estimate their properties. One of the main advantages of GNSS-R, when compared with the conventional methods, is the intermediate coverage area, as well as, the use of the well-defined structure of GNSS systems that guarantee appropriate temporal resolution. The scope of this paper is to present a conceptual review of GNSS-R applied to soil moisture monitoring.

**Keywords:** GNSS-R. Multipath. Soil Moisture. SNR.

**Resumo**: O monitoramento da umidade do solo possibilita o manejo e uso eficiente de recursos hídricos, sendo uma atividade importante em diversas áreas, tais como: no monitoramento de áreas de risco; delimitação de áreas suscetíveis a enchentes; atividades da geotecnia; e na agricultura. A Refletometria GNSS (GNSS-R) é um desenvolvimento científico e tecnológico que permite realizar sensoriamento remoto ou proximal, a depender da altura da antena em relação à superfície, com satélites de navegação. Neste método, explora-se os sinais GNSS que chegam à antena receptora de maneira direta e indireta, após reflexão nas superfícies existentes no entorno da antena. A combinação destes dois sinais ocasiona o efeito de multicaminho, que afeta as observáveis GNSS e deteriora o posicionamento. Por outro lado, ao interagir com estas superfícies, o sinal indireto permite estimar atributos acerca destas superfícies, como por exemplo a umidade do solo. Uma das principais vantagens em relação aos métodos convencionais reside no fato do GNSS-R proporcionar uma área de abrangência intermediária e o uso da estrutura bem estabelecida dos satélites GNSS, que garantem resolução temporal apropriada. O escopo deste trabalho é apresentar uma revisão conceitual acerca do GNSS-R aplicado no monitoramento da umidade do solo.

**Palavras-chave:** GNSS-R. Multicaminho. Umidade do Solo. SNR.

# 1   INTRODUCTION

Soil moisture can be defined as the water content stored in the unsaturated soil zone, also termed the vadose zone (HILLEL, 1998). The vadose zone contains the root zone of the plants and extends from the land surface to the groundwater table of the first unconfined aquifer, where all soil pores are filled with water (ARORA et al., 2019).

Soil moisture content is inhomogeneously distributed vertically (over depth) and horizontally (over land) (SENEVIRATNE et al., 2010). This quantity is commonly expressed for a given portion of soil at a given matric potential in gravimetric or volumetric units (TULLER; OR, 2004). Gravimetric soil moisture (g/g) is the ratio between the mass of the water within a soil sample and the dry mass of the soil sample. Volumetric soil moisture is the ratio between the volume of water contained in a given volume of a soil sample (cm³/cm³) (BABAEIAN et al., 2019).

Soil moisture is linked to processes that are characterized at various scales. At large scales it is a key component of the water and biogeochemical cycles, as well as influencing the flow and exchange of energy between the Earth's physical surface and the atmosphere (ENTEKHABI et al., 2010; ROBINSON et al., 2008). Within the scope of the water cycle, quantifying soil moisture allows inputting models for the delimitation of aquifer recharge areas and flood areas (OCHSNER et al., 2013). The water stored on land is a relevant agent in mass displacements, thus soil moisture is an important parameter in systems for monitoring areas susceptible to natural hazards; in geotechnical activities; and in the planning and control of engineering works. Locally, soil moisture has critical importance in agriculture, for example, because it is essential for the healthy development of plants. Monitoring soil moisture allows optimizing the use of water and energy resources in irrigation mechanisms (PEREIRA, 2001). In this way, its management contributes to the increase in production and, concomitantly, the preservation of the environment.

Global Navigation Satellite System Reflectometry (GNSS-R) has been successfully used in soil moisture estimation (Table 1), emerging as an alternative to conventional methods (Section 2). This method allows the realization of remote or proximal sensing exploring the reflections of the radio waves transmitted by GNSS satellites. It makes it possible to extract information on the properties of the reflecting surfaces (TEUNISSEN; MONTENBRUCK, 2017), such as soil moisture. GNSS-R has certain advantages over other methods, including global coverage; low cost; independence from climatic conditions; the possibility of obtaining information almost in real-time; and the short revisit time of GNSS satellites (EDOKOSSI et al., 2020). In the present paper, a conceptual review of the GNSS-R method for estimating soil moisture is presented.

# 2   CONVENTIONAL METHODS

There exist several methods to measure or estimate soil moisture, directly or indirectly (SENEVIRATNE et al., 2010). In the gravimetric method, soil moisture content is directly measured. In the laboratory, soil moisture content can be derived weighting an *in situ* soil sample before and after drying. The original volume of water in the soil sample is calculated by dividing the water mass by its density (HANSON, 2009). The gravimetric method is the most accurate method and the only direct method. It represents the reference measurements for calibrating equipment used in indirect methods (MENDES, 2006). However, it provides punctual measurements, which may not be representative of the larger surrounding area at a local scale. Besides, it is laborious and destructive, due to the need to collect soil samples (ZHANG et al., 2014). Therefore, it may not be suitable for continuous monitoring.

In all other methods, soil moisture is indirectly estimated from measurement of physical properties of the soil. In these cases, measurements can be made by *in situ* probes or by remote or proximal sensing (BABAEIAN et al., 2019). Probes are autonomous and allow ample data recording, allowing continuous monitoring. The main property explored by these types of equipment is the dielectric permittivity of the soil. The two most common techniques among probes that measure electric permittivity of the soil are based on the

Time Domain Reflectometry[1] (TDR) and Frequency Domain Reflectometry (FDR), also termed capacitance probes (SENEVIRATNE et al., 2010). In TDR probes, permittivity is determined by evaluating the variation in the propagation time of an electromagnetic pulse. In turn, in FDR probes, permittivity is estimated by assessing the frequency variation of an electromagnetic pulse (LIMA; SILVA; KOIDE, 2012). These probes are accurate, but limited in terms of range, which is a few centimeters around the sensor. The capacitance probes have limitations related to soil composition, mainly due to the content of salinity and iron oxides (DELTA-T DEVICES LTD, 2001).

Furthermore, one can evaluate the moderation of fast neutrons, which is linked to the presence of hydrogen atoms. Neutron probes can be active or passive. The active probes have their radiation source, mainly from Americium and Beryl, to give rise to fast neutrons (PEREIRA, 2001). They have the disadvantage of biological risks to the equipment operator and the environment due to the emission of ionizing radiation. Passive probes explore radiation from extraterrestrial sources that originate from galactic cosmic rays. When these rays reach the atmosphere, they give rise to a cascade of neutrons with high energy. These neutrons continue to propagate downward reaching the soil, when a second cascade of neutrons arises. These neutrons are moderated by hydrogen atoms contained in water that characterizes the soil moisture (DESILETS; ZREDA; FERRÉ, 2010). The probes of the COsmic-ray Soil Moisture Observing System (COSMOS) network exploit this property (ZREDA et al., 2012). They have a range of hundreds of meters, are accurate, and allow ample and autonomous data recording; however, they can be expensive. On the other hand, through orbital and aerial remote sensing, global or regional coverage can be reached, respectively, but with generalized information (VEY et al., 2016).

The spatial resolution obtained with orbital sensors is approximately 100 m for active sensors (radars) and 10 km for passive sensors (radiometers) (EDOKOSSI et al., 2020). Also, the temporal resolution, which is related to the satellite revisiting the same location, is low. These characteristics limit its use in applications such as agriculture. Electromagnetic waves of different spectrum bands from visible to microwaves can be used in remote sensing through active and passive sensors. Some examples of satellite missions for monitoring soil moisture are the European Space Agency's Soil Moisture and Ocean Salinity satellite (SMOS) of (KERR et al., 2001) and National Aeronautics and Space Administration's Soil Moisture Active Passive (SMAP)(ENTEKHABI et al., 2010). Both employ radio waves with active and passive sensors. Other missions in this theme include: Special Sensor Microwave/Imager (DE RIDDER, 2003), Tropical Rainfall Measuring Mission (GAO et al., 2006), Advanced Microwave Scanning Radiometer – Earth Observing System (XIE; MENENT; JIA, 2019), and gravimetric missions such as the Gravity Recovery and Climate Experiment (SWENSON et al., 2008).

## 3    GNSS REFLECTOMETRY

Several studies have demonstrated that soil moisture can be estimated by GNSS-R (Section 4). In addition to the results obtained by these researchers demonstrating the efficiency of GNSS-R in this purpose, some advantages can be highlighted: 1) intermediate coverage area, between conventional methods (*in situ* probes and remote sensing) – approximately 50 meters radius for a 2-m tall GNSS antenna (TABIBI et al., 2017); 2) adequate spatial and temporal resolution guaranteed by the existing GNSS structure, which has global coverage, continuous transmission of signals by dozens of satellites, independently to weather conditions (SEEBER, 2003); 3) possibility of using GNSS stations simultaneously for positioning and reflectometry (LARSON; NIEVINSKI, 2013).

GNSS satellites transmit electromagnetic waves of the radio or microwave type with frequency in the range of 1 to 2 GHz, in the L band (TEUNISSEN; MONTENBRUCK, 2017). Coincidentally, these frequencies are close to the frequencies used in SMOS and SMAP orbital missions. When such waves reflect on surfaces around a GNSS antenna, they can reach this antenna indirectly (Figure 1) delayed due to the additional distance traveled (LEICK, 1995). The combination between direct and reflected waves gives rise to the multipath effect,

---

[1] Note the conceptual distinction between these conventional methods of indirect measurement of soil moisture Time Domain Reflometry (TDR) and Frequency Domain Reflometry (FDR), and the GNSS-R geodetic method, which is based on GNSS transmissions.

which is one of the main sources of errors that affect GNSS positioning, depending on the quality of the antenna (TEUNISSEN; MONTENBRUCK, 2017).

After the interaction with the ground surface, radio waves have their characteristics changed (amplitude, phase, polarization, and frequency). This makes it possible to estimate attributes about those reflection surfaces (ROUSSEL et al., 2016). This is the principle of remote sensing, including GNSS-R that exploites the GNSS observables affected by reflections. In this way, multipath enables GNSS-R, despited being detrimental to GNSS positioning, thus expanding the range of applications of this technology.

Figure 1 – Simultaneous reception of direct and indirect waves from reflections on the surfaces surrounding a GNSS antenna.
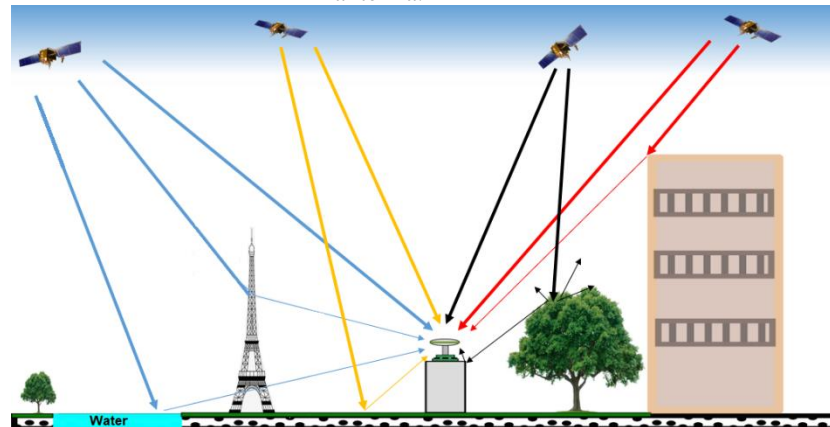


Source: Euriques (2019).

GNSS-R can be considered as a multi-static radar since the antenna receives multiple transmissions from several satellites (JIA; PEI, 2018). This configuration contrasts with monostatic radars, where receivers and transmitters are on the same platform, as in the case of nadir-pointing satellite altimeters. Although the concept of GNSS Reflectometry was initially proposed by Martin-Neira (1993), most of the related research comes from the last decade. Applications involve the determination of geometric attributes and the composition of reflective surfaces. Altimetry is considered in the first type and consists of determining the vertical distance between the GNSS antenna and the reflection surface as in snow depth monitoring (ZHOU et al., 2019), water level variations (STRANDBERG; HOBIGER; HAAS, 2017), and some types of vegetation growth (ZHANG et al., 2017). The application type dealing with surface composition includes soil moisture estimation (TABIBI et al., 2015).

Multipath affects all observables, so GNSS-R can be performed, in principle, through pseudorange, Doppler, carrier phase, or Signal-to-Noise Ratio (SNR) data. According to Nievinski and Larson (2014a) and Larson et al. (2010), SNR consists of the power of the carrier phase (in watts) normalized by the noise power or its spectral density (watts or watts per hertz), often expressed in a logarithmic scale, in decibels (dB) or decibel-hertz (dB-Hz). This observable is recorded continuously by GNSS receivers throughout the tracking, considering each satellite individually (BILICH; LARSON, 2007).

With the orbital movement of satellites, the propagation delay and the phase difference between direct and reflected signals varies, creating constructive and destructive interference patterns between the two superimposed waves, in turn resulting in oscillations (Figure 2) in the SNR time series (TABIBI et al., 2015). SNR is the GNSS observable that best reveals the multipath effect, as it is invariable to the common effects between the direct and indirect paths, even with single frequency receivers, such as errors related to orbits, most of the atmospheric delays and synchronization errors, which would affect the other GNSS observables (LARSON et al., 2008a). In comparison, carrier phase and pseudorange observables require combinations of two or three carrier frequencies to isolate the multipath effect. In any case, it is possible to perform reflectometric determinations from conventional GNSS receivers, developed for positioning, without changes to the equipment or installation of the receiving antenna (LARSON et al., 2010). In this context, data from existing GNSS stations can be used, such as from the Brazilian Network for Continuous Monitoring of GNSS (RBMC), the continuous monitoring network from the Geocentric Reference System for the Americas

Rev. Bras. Cartogr, vol. 73, n. 2, 2021

DOI: http://dx.doi.org/10.14393/rbcv73n2-55033

(SIRGAS), or from the International GNSS Service (IGS).

Different names can be found in the literature about the category of GNSS-R that exploits conventional ground instruments, developed for positioning and adapted to reflectometry: GNSS Multipath Reflectometry (GNSS-MR) by Nievinski et al. (2016); GNSS Interference Pattern Technique (GNSS-IPT) by Rodriguez-Alvarez et al. (2011a); GNSS Interferometric Reflectometry (GNSS-IR) by Larson (2016); SNR-based GNSS reflectometry by Löfgren and Haas (2014). GNSS-MR can be performed with any GNSS observable, while GNSS-IPT/IR is normally restricted to the use of the SNR-type observable.

Access to SNR can be done in two different ways:

a)      observation file in Receiver Independent Exchange (RINEX) format, which allows different types of SNR for each carrier frequency (GURTNER; ESTEY, 2015). Since version 3, SNR values are provided for each modulation at the same frequency (e.g., civil and military)

b)      National Marine Electronics Association (NMEA) 0183 format, which is the specification related to data standardization for communication between electronic equipment (MARTÍN et al., 2020). This specification includes the transmission of SNR data via the GPS Satellites in View message ($GPGSV).

Figure 2 shows an SNR interferogram for different modulations, considering the ascending arc of a satellite in the GPS constellation. Note that not all signals have the same quality concerning the multipath signature. In general, modern GPS modulations, such as L2C and L5, correspond better to theoretical models, while legacy modulations, such as C/A and P(Y) exhibit more distortions (TABIBI et al., 2017).

Figure 2 –SNR (dB) by different modulations for an ascending arc of a GPS satellite considering elevation angles between 5 and 45 degrees.
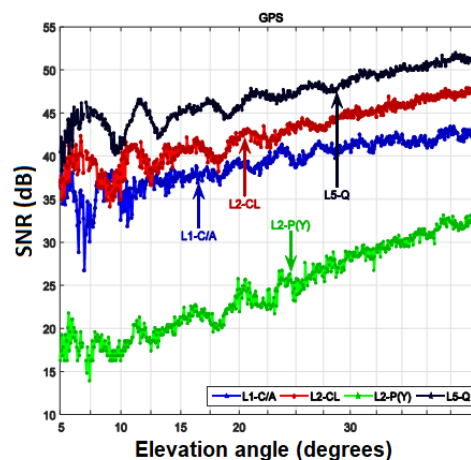


Source: Adapted from Tabibi et al. (2017).

## 3.1   GNSS-R footprint

The coverage area involved in GNSS-R is defined mainly as a function of the height ($H$) of the antenna above the surface. In this sense, the range is local, when GNSS stations are mounted a few meters above the ground (LARSON et al., 2008a); regional, when the receiving antenna is fixed on airborne platforms such as conventional and remotely piloted aircraft (RODRIGUEZ-ALVAREZ et al., 2013); or global, when the sensor is fixed on orbital platforms (GLEASON et al., 2005).

The coverage area for stations installed on the ground can be approximated by the Fresnel zones. Each one of the Fresnel zones is an ellipse defined in terms of the elevation angle ($e$) and azimuth ($a$) over the horizon of the antenna (Figure 3) (JIN; QIAN; KUTOGLU, 2016). In this calculation, the height of the antenna and the wavelength ($\lambda$) of GNSS carrier wave must also be considered. Following Larson and Nievinski (2013) and assuming a flat and horizontal surface, the formulation for the first Fresnel zone can be expressed in terms

of its semi-major (*a*) and semi-minor axes (*b*) as well as the horizontal distance to the center (*D*):

$$a = \frac{b}{\sin e} \tag{1}$$

$$b = \sqrt{\frac{2dH}{\sin e} + \frac{d^2}{\sin^2 e}} \tag{2}$$

$$D = \frac{H}{\tan e} + \frac{d}{\sin e \tan e} \tag{3}$$

where $d = 0.5\lambda^{-1}$. The major semi-axis is positioned along the satellite's azimuth.

Figure 3 shows the Fresnel zones of a GNSS station with an antenna height of 1.8 meters. On the left, the Fresnel zone of a satellite with 90 ° azimuth is shown. The ellipses for different elevation angles are shown; the higher the elevation angle (closer to the zenith), the smaller and closer to the antenna is the ellipse. On the right, there is the set of Fresnel zones for a station assumed in the Southern Hemisphere. Note the absence of zones in the vicinity of the South direction, which occurs due to the inclination of the orbital plane of satellites (LARSON, 2016). When the GNSS station is located in the Northern Hemisphere, this gap occurrs in the northern direction.

Figure 3 – Fresnel zones of a simulated GNSS station considering satellite elevation angles between 7 e 25 degrees from the antenna horizon
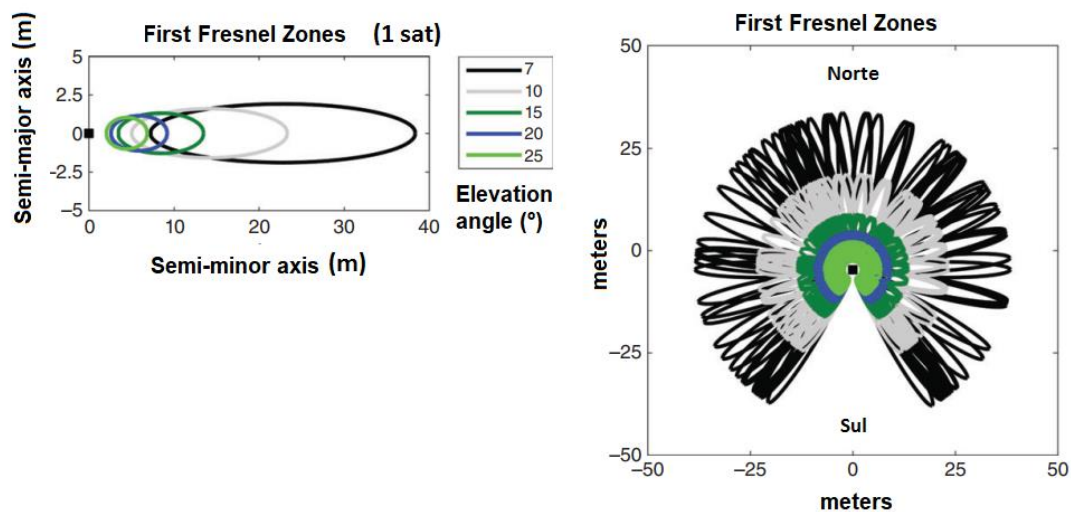


Source: Adapted from Larson (2016).

## 3.2 Reception of reflected signals

Indirect signals (reflected waves) are received by the antenna mainly from its lower hemisphere. The GNSS antennas are designed to aim at the rejection or mitigation of the reflected waves. In this context, it is common to use a metal plate integrated into the antenna element, named ground plane, or the use of a special antenna attachment made of concentric metal rings named choke rings (MONICO, 2008). Specific configurations were developed to increase the reception of these reflected waves (JIA; PEI, 2018):

a)      Two antennas: one of them oriented in a conventional way, towards zenith, aiming to receive direct waves, and another antenna oriented to nadir, or close to it, to capture the reflected waves. This was the first configuration proposed for GNSS-R (MARTIN-NEIRA, 1993). This configuration is not compatible with GNSS-MR/IPT/IR, because conventional GNSS receivers are unable to track the two

waves separately. See Figure 4a;

b)    Single vertical antenna: This is the case with only one antenna oriented towards zenith (conventional orientation to GNSS positioning). It simultaneously receives direct and reflected waves (Figure 4b.) This configuration allows the shared use of the GNSS station for positioning and reflectometry (LARSON et al., 2008a);

c)    Single tilted antenna: analogous to the previous case, however with the antenna pointed at the horizon, or close to it (Figure 4c) (RODRIGUEZ-ALVAREZ, 2009). It has the advantage of amplifying the reception of waves reflected in the target azimuth; as a disadvantage, it impairs reception in the opposite azimuth.

Figure 4 – Antenna system schemes in GNSS-R.
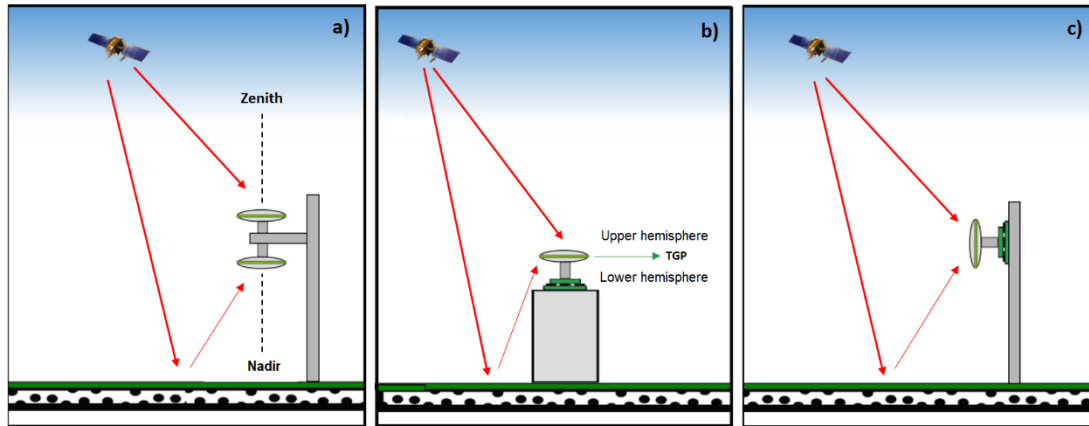


Source: The authors (2021).

## 3.3   SNR Modeling

The modeling of SNR for reflectometry purposes is carried out through the combination of a physical model, related to the theoretical simulation of the multipath (NIEVINSKI; LARSON 2014b), and an inverse model, by which unknown parameters are estimated through GNSS measurements (NIEVINSKI; LARSON, 2014c).

### 3.3.1   PHYSICAL MODEL: THEORETICAL SIMULATION

The scattering of electromagnetic waves occurs in three ways: diffraction, specular (coherent reflection), and diffuse (incoherent reflection) (ZAVOROTNY et al., 2015). These conditions occur mainly due to the characteristics of the reflecting surfaces. Specular reflections are the ones that most interfere with direct waves since only coherent waves are subject to superposition. Coherent observations maintain a stable phase relationship between direct reflected waves (NIEVINSKI; MONICO, 2016). In contrast, incoherent observations have a random phase and do not maintain a predictable relationship between these waves.

The GNSS satellite transmissions are Right-Hand Circularly Polarised (RHCP) (WU; JIN, 2019). When reflecting on surfaces, two components can be generated, RHCP and Left-Hand Circularly Polarised (LHCP) (KATZBERG et al., 2006). The proportion between these components depends on the direction of incidence of the direct wave and the dielectric properties of the reflecting surface. The electric field of the reflected wave ($\overline{E_r}$), in volts per meter, is a complex vector, therefore with magnitude and phase given according to Eq. (4) (NIEVINSKI; LARSON, 2014a):

$$\overline{E_r} = S \cdot I \cdot \overline{\overline{R}} \cdot \overline{E_d} \tag{4}$$

where $\overline{E_d}$ is the direct field. The magnitude $S$ represents a loss of coherent power due to the surface roughness, $S = \exp\left(-2\pi^2\lambda^{-2}\sigma_h^2\sin^2 e\right)$, which is a real value and less than 1; $\sigma_h$ is the surface height standard deviation

(in meters). The scalar $I = \exp\left(2\pi\lambda^{-1}\tau_i\sqrt{-1}\right)$ is a complex value, usually unitary, which involves the phase difference resulting from the propagation delay ($\tau_i$, in meters) between reflected and direct waves. For a flat and horizontal surface, $\tau_i$ (Eq. (5)) can be estimated as a function of the satellite's elevation angle and antenna height (GEORGIADOU; KLEUSBERG, 1988):

$$\tau_i = 2H\sin(e) \tag{5}$$

In Eq. (5), $H$ is the vertical distance between the antenna phase center and the reflecting surface (TABIBI et al., 2015); it is not exactly the geometric height of the antenna above the ground surface, as it depends on the penetration depth of the electromagnetic wave.

The reflection matrix $\bar{\bar{R}}$ (Eq. (6)), represents the effect of the surface composition on the reflected electromagnetic wave (NIEVINSKI; LARSON, 2014a):

$$\bar{\bar{R}} = \begin{bmatrix} R^S & R^X \\ R^X & R^S \end{bmatrix} \tag{6}$$

This matrix is determined by the combination of the circularly polarized scalar reflection coefficients (complex values): $R^S$ (Eq. (8)) for the same-sense polarizing value and $R^X$ (Eq. (9)) the cross-sense polarizing value (NIEVINSKI; LARSON, 2014a).

Although the direct electric field has only RHCP component ($E_d^R$) due to negligible LHCP component ($E_d^L \approx 0$), the reflected field can have both non-zero components ($E_r^R$, $E_r^L$). In the case of GNSS, Eq. (4) can be simplified as Eq. (7):

$$\overline{E_r} = [E_r^R, \quad E_r^L]^T = S \cdot I[R^S, \quad R^X]^T E_d^R \tag{7}$$

The circularly polarized scalar reflection coefficients are defined based on the linearly polarized reflection coefficients that follow from the Fresnel equations (NIEVINSKI; LARSON, 2014a):

$$R^S = \frac{R^H + R^V}{2} \tag{8}$$

$$R^X = \frac{R^H - R^V}{2} \tag{9}$$

These coefficients are complex values that depend on the angle of incidence of the wave. In general, the same-sense polarized reflection tends to zero for normal incidence (perpendicular to the surface), while cross-sense polarized reflection tends to zero for near-grazing incidence. In the case of GNSS, this means that high satellites tend to have LHCP reflections, and low satellites tend to have RHCP reflections. Therefore, for satellites close to the zenith, the reception of reflection signals would be better with an antenna with LHCP polarization.

In Eq. (8) and Eq. (9), the coefficients on the right side of the equalities are the linear vertical ($R^V$) and linear horizontal ($R^H$) reflection coefficients (NIEVINSKI; LARSON, 2014a):

$$R^V = \frac{(\cos\theta - \sqrt{\varepsilon - \sin^2\theta})}{(\cos\theta + \sqrt{\varepsilon - \sin^2\theta})} \tag{10}$$

$$R^H = \frac{(\varepsilon \cdot \cos\theta - \sqrt{\varepsilon - \sin^2\theta})}{(\varepsilon \cdot \cos\theta + \sqrt{\varepsilon - \sin^2\theta})} \tag{11}$$

where $\theta = 90° - e$ (assuming flat surface). The complex dielectric constant ($\varepsilon = \varepsilon' + \sqrt{-1}\varepsilon''$) of the medium is a complex number with real ($\varepsilon'$) and imaginary ($\varepsilon''$) components that are related to the medium conductivity (EDOKOSSI et al., 2020). In the case of soil, the values of those components vary with moisture according to empirically calibrated curves (Figure 5), which link relative permittivity (adimensional) and moisture for different types of soil (HALLIKAINEN et al., 1985).

The indirect electric field exists only in the free space between transmitting satellite and receiving antenna (TABIBI et al., 2015). Consequently, it is necessary to calculate the electrical voltage (volts) of the direct ($V_d$) and reflected waves ($V_r$) induced in the electrical connection between antenna and receiver. This is done by multiplying the electric field vector by the antenna effective length ($\bar{L}$), a complex vector in meters:

$$V_d = E_d^R \cdot L_d^R \tag{12}$$

$$V_r = L_r^R \cdot E_r^R + L_r^L \cdot E_r^L = S \cdot I \cdot X \cdot E_d^R \tag{13}$$

Note that there are components for both polarizations (RHCP ou LHCP), denoted by superscript letters. The subscript denotes the direction of the reception (direct or reflected signal) e.g., $L_d^R$ is the antenna response for a direct RHCP wave. The magnitude and argument of each $\bar{L}$ the component comes, respectively, from the gain pattern and the phase center variations of the antenna, both previously calibrated. The factor $X = L_r^R R^S + L_r^L R^X$ represents the interaction between the antenna responses ($L$) and the reflecting surface response ($R$) (TABIBI et al., 2015). Therefore, it is linked to the soil moisture of the reflected surface.

Figure 5 – Complex components of soil permittivity for different types of soil at a 1.4 GHz frequency.
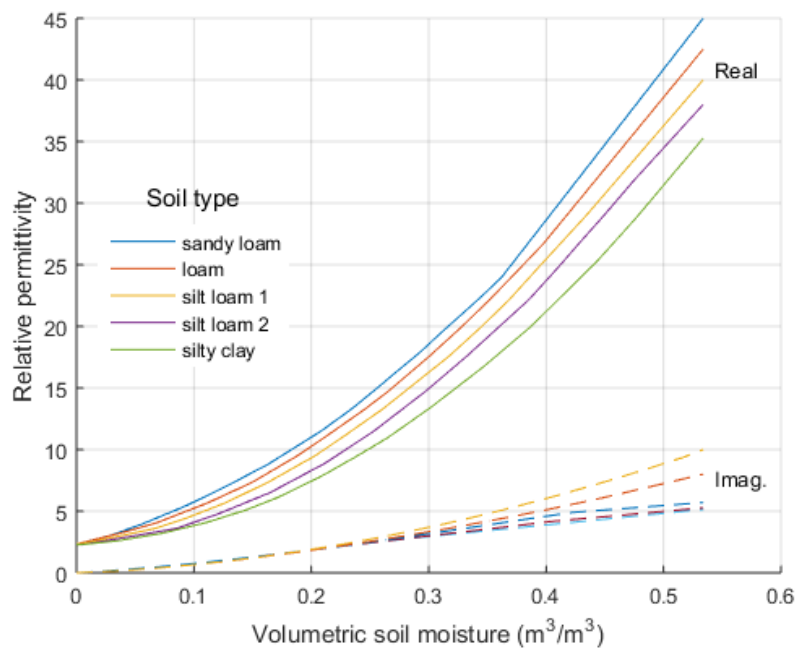


Source: Adapted from Hallikainen et al. (1985).

Finally, the composite voltage, resulting from the superimposition of direct and reflected waves, can be obtained: $V = V_d + V_r$. This sum occurs on the complex plane, separately for the real and imaginary components. The corresponding power $P = V^2$, in watts, is given by:

$$P = P_d + P_r + 2\sqrt{P_d}\sqrt{P_r}\cos\phi_i \tag{14}$$

$P$ is related to the powers of the direct signal ($P_d = |V_d|^2$) and the reflected signal ($P_r = |V_r|^2$). It also includes a trigonometric term dictated by the interferometric phase ($\phi_i$), the difference between the phases of the two

voltages: $\phi_i = \phi_r - \phi_d = \arg(V_r) - \arg(V_d)$ (NIEVINSKI; LARSON, 2014a). The interferometric phase is dominated by the propagation delay ($\tau_i$) stemming from the additional path of the reflected signal (TABIBI et al., 2015), which is given by Eq. (15):

$$\phi_i \cong 2\pi\lambda^{-1}\tau_i + \phi_X = 2\pi\lambda^{-1}2H\sin(e) + \phi_X \tag{15}$$

This equation includes the compositional phase $\phi_X = \arg(X)$, resulting from the combination of the properties of the reflecting surface and the GNSS antenna (NIEVINSKI; LARSON, 2014a). This is the phase component that depends on soil moisture. It varies with the satellite's elevation angle as the reflected wave changes polarization. Figure 6a shows the relationship between these quantities in two theoretical scenarios: the first is completely dry soil (blue); the second with soil moisture equals 50% (red). Following Liu and Larson (2018), the variations in the compositional phase cause a bias in the geometric height, designating a compositional height bias $H_X = \partial\phi_X/\partial k_z$, given by the rate of change in $\phi_X$ with respect to vertical wavenumber, $k_z = 4\pi\lambda^{-1}\text{sen}(e)$. Figure 6b shows the simulated height bias as a function of elevation angle in the two soil moisture scenarios.

Figure 6 – Compositional phase ($\phi_X$) on the left panel and compositional height bias on the right, as a function of the satellite elevation angle in two scenarios concerning soil moisture (0 e 50%).
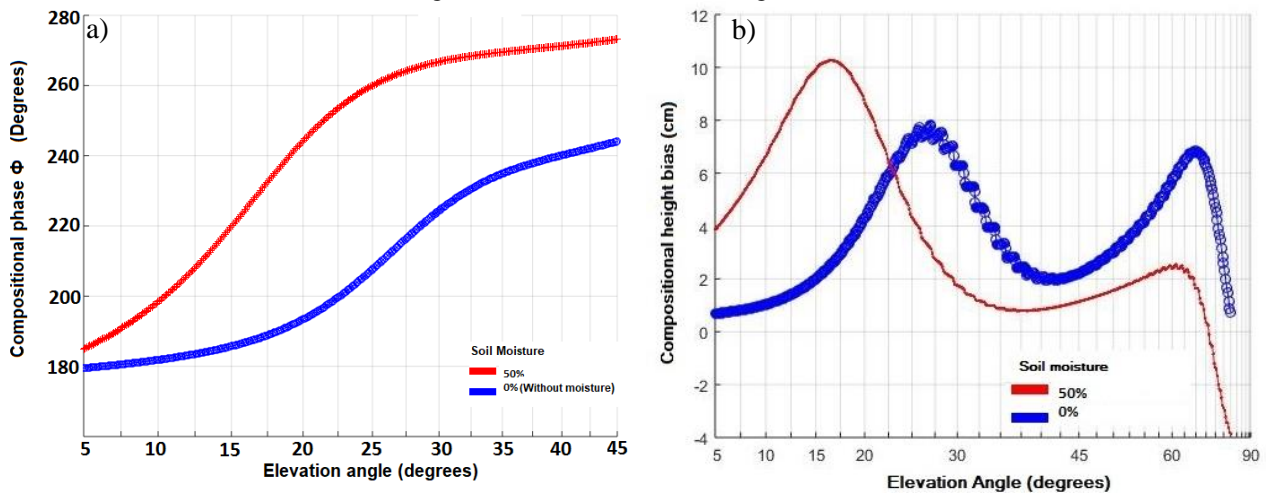


Source: The authors (2021).

Figure 7 – SNR (dB) simulated for two scenarios: without soil moisture (blue); soil moisture 50% (red).
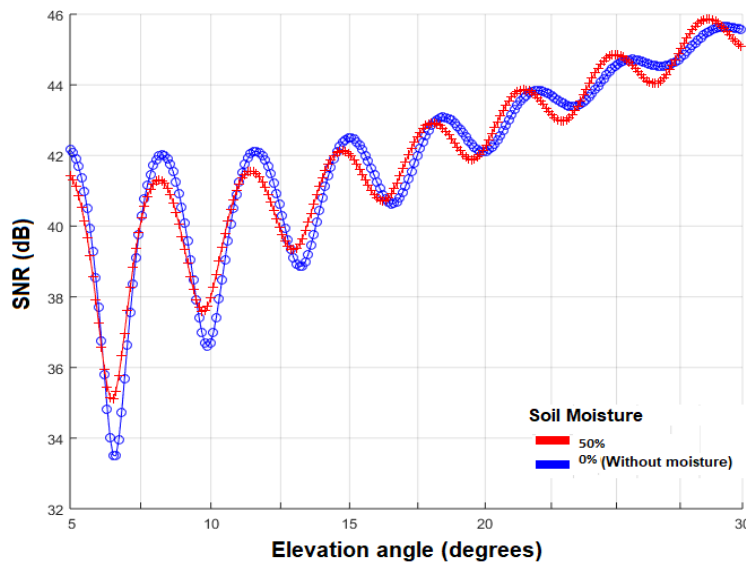


Source: The authors (2021).

According to Nievinski and Monico (2016), when the input signal is received, its power ($P$) is normalized by the noise power ($P_n$) and recorded by the receiver. $P_n$ is an arbitrary constant in the context of $SNR = P/P_n$, in watts per watts. The observed ratio can be modeled as the sum of two components, $SNR = tSNR + dSNR$: a trend ($tSNR$) and a detrended ($dSNR$) interference fringes term (TABIBI et al., 2017). The trend $tSNR = P_n^{-1}(P_d + P_r)$, stems mainly from the antenna gain pattern and has a polynomial form. The complementary component $dSNR = 2P_n^{-1}\sqrt{P_d}\sqrt{P_r}\cos\phi_i$, resulting from the in-phase and out-of-phase alignment of direct and reflected waves, has a sinusoidal form (NIEVINSKI; LARSON, 2014c). Figure 7 shows two SNR simulations generated from the forward modeling (theoretical simulation).

### 3.3.2    EMPIRICAL MODEL: SINUSOIDAL FIT

The physical model (section 3.3.1) can be approximated by the empirical model of Eq. (16). In this equation, $k_z$ is adopted as an independent variable, because it is the basis of the propagation delay $\phi_i = k_z H + \phi_X$, assuming a flat, horizontal surface (ZAVOROTNY et al., 2010).

$$tSNR \approx (c_0 + c_1 k_z + c k_z^2 + \cdots)$$
$$dSNR \approx A_m \cdot \cos(H_m k_z + \phi_m)$$

(16)

The parameter $H_m$ is related to the multipath oscillation frequency. The sum $\sum c_i k_z^i$, is a polynomial that approximates the trend; and the sinusoid approximates the dSNR complement. The amplitude $A_m$ (Eq. (17)), the initial phase $\phi_m$ (Eq. (18)) and the effective height $H_m$ (Eq. (19)), are given following by Nievinski and Larson (2014c):

$$A_m \approx E\{2P_n^{-1}\sqrt{P_d}\sqrt{P_r}\}$$

(17)

$$\phi_m \approx E\{\phi_X - k_z H_m\}$$

(18)

$$H_m \approx H + E\{H_X\}$$

(19)

These empirical parameters ($A_m$, $\phi_m$ and $H_m$) are constants defined from the expectation $E\{\cdot\}$ of the variables resulting from the rigorous formulation of the theoretical model. The compositional height bias $H_X$ ends up assimilated in the effective height $H_m = H + H_X$ (Figure 6b) (NIEVINSKI; LARSON, 2014a). In turn, the empirical phase $\phi_m$ is the average of the residual compositional phase, $\phi_X - k_z H_m$.

The parameters $A_m$, $\phi_m$ e $H_m$, observed in SNR observations, vary depending on factors such as carrier wavelength, free-space propagation medium, and the equipment, besides the influence of the reflected signal. Each of these empirical parameters responds better to a given application. The empirical height $H_m$ has been applied for altimetric applications as sea level monitoring and snow depth. In turn, the empirical amplitude $A_m$ has been applied in vegetation growth monitoring (SMALL et al., 2016) and sea waves, because such phenomena affect the surface roughness. The empirical phase $\phi_m$ parameter has been employed on soil moisture estimations (CHEW et al., 2014).

### 3.3.3    INVERSE MODEL: STATISTICAL MODEL

The physical and empirical models can be ideally combined using previously available information, such as the antenna model and the type of soil, estimating as unknowns only the effects that vary with time, such as soil moisture. This strategy was developed and applied initially for the measurement of snow depth (NIEVINSKI; LARSON, 2014c, 2014d). Afterward, it was adapted for use in determining soil moisture (TABIBI et al., 2015). The inversion is a statistical model through which the unknown parameters are determined from the GNSS observations. These measured observations are compared internally with the

observations simulated by the forward physical model (NIEVINSKI; LARSON, 2014b). Hence, the simulated observations are fitted to the measurements, involving in this process a nonlinear least-squares adjustment of the unknown parameters (NIEVINSKI; LARSON, 2014c). As a result, we have the estimated parameters and their precision: amplitude, phase, antenna height, and polynomial coefficients of the trend.

### 3.3.4    POST-PROCESSING: PHYSICAL-STATISTICAL COMBINATION

After inversion, several post-processing measures are required. Through this module, the inversion parameters are subjected to statistical inferences, quality control, and optimization of results (NIEVINSKI; LARSON, 2014d). Figure 8 shows simulated SNR observables and measured observations, as well as the residuals associated with the difference between these observables.

In the case of soil moisture, the phase parameters (phase shift and the respective phase rate) have their precision degraded, as they are very correlated. As soil moisture content affects the penetration depth of electromagnetic waves into the soil, this creates variations in the effective height of the antenna (LARSON, 2016). Thus, a strategy to improve the estimation of the phase parameters is to define an average value for this height and introduce it as a constraint in post-processing (EURIQUES, 2019).

It is also necessary to combine the independent estimates of the various satellites into an average value for the station. Finally, a calibration curve, using a first or second-degree polynomial, establishes the relationship between the parameters of the interferometric phase with the soil moisture values. Figure 9 exemplifies the relationship between phase values (vertical axis) and soil moisture (horizontal axis). In this figure, the phase values were estimated from the reflected waves of the GPS satellite PRN 29 at a given station, whereas soil moisture values were determined by the average of 5 TDR probes located close to this station (LARSON et al., 2008b).

Figure 8 – Simulated and measure SNR signature and its residues for an ascending arc for the PRN02 satellite.
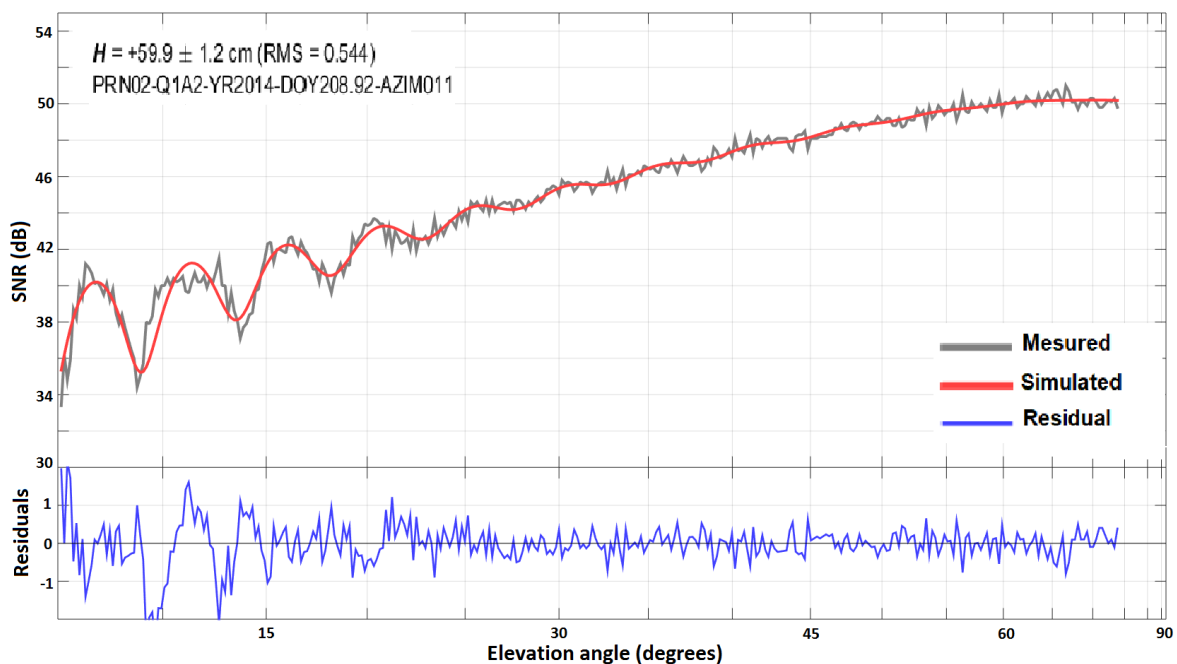


Source: The authors (2021).

Figure 9 – Relationship between reflectometric phase and soil moisture.
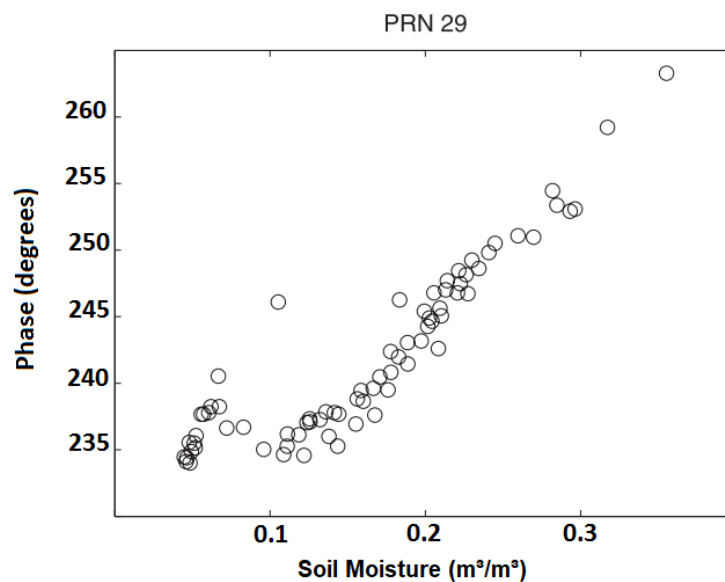


Source: Adapted from Larson et al. (2008b).

The calibration curve between soil moisture and the phase-shift is based on linear regression in the form $a \cdot \phi_m + b$, whose slope is often reported in the literature as $a = 1,48 \ \mathrm{cm^3 cm^{-3 \circ -1}}$ (CHEW et al., 2015) or its reciprocal, $a^{-1} = 65°/(\mathrm{cm^3/cm^3})$ (VEY et al., 2016). These values were determined from physical simulations considering specific antenna models. The intercept or constant coefficient of the regression ($b$) is associated with residual soil moisture, which represents the minimum value present in the soil. It is normally assumed $b = 0,05 \ \mathrm{m^3 m^3}$ (VEY et al., 2016). Following Chew et al. (2015), the coefficient $b$ can also be obtained through the interpolation of soil texture maps.

## 3.4 Method limitations

The two coefficients of phase calibration for soil moisture are dependent on the site location and the GNSS antenna model; therefore, they are uncertain for locations without additional data from conventional methods or that have had an antenna exchange. This is probably the largest limitation of using the GNSS-R method to soil moisture monitoring. Other limitations must be considered such as the effects of topography, vegetation, surface roughness, and soil temperature because they affect the determinations.

Ground vegetation may obstruct the incidence and reflection of radio waves on the ground (ZHANG et al., 2017). Besides, as explained in section 3.3.2, vegetation influences the roughness of the reflection surface, which can affect the coherence of the signals and the amplitude and phase determinations. Furthermore, the location of the GNSS station and the characteristics of the surroundings should have unobstructed visibility to the ground on the reflection area, avoiding objects like fences, which is a basic condition for carrying out GNSS-R.

Another limitation, not only for GNSS-R but also for other remote sensing methods that use microwaves (L, C, and X bands), concerns the power of penetration of these electromagnetic waves into the ground, which in the case of GNSS frequencies is mainly limited to a depth of about 5 cm (EDOKOSSI et al., 2020). Thus, considering that the soil moisture varies along with a vertical profile in the soil when making statistical comparisons between different methods, one should consider these possible differences between the reference depths of each method.

## 4 RELATED STUDIES

In this section, we highlight the main works in which soil moisture was estimated through GNSS-R using SNR from ground stations. Table 1 lists information such as: authorship; antenna height about the ground

(meters); duration (days); GNSS system: being GPS (G), GLONASS (R), BeiDou (B), or Galileo (E); GNSS modulation; soil cover; method of validating the reflectometric determinations; as well as the correlation (in percentage).

Other types of GNSS-R, such as from aerial and orbital platforms, are not discussed. Further details can be found, for example, in: Jin, Cardellach and Xie (2014); Masters, Axelrad and Katzberg (2004); Chew and Small (2018); and Eroglu et al. (2019).

Larson et al. (2008a) were the pioneers in this theme. They have detected correlations between the time series of reflected signal amplitudes, obtained by SNR via RINEX, and soil moisture obtained by the Noah Land Surface Model. This model allows evaluating the evolution of moisture using meteorological parameters as input data. GPS data recorded at the TASH station, located in Tashkent, Uzbekistan, were used. The surroundings of this station are covered by low vegetation (grass). The effects of vegetation on the modeling of reflective signals were not considered. To determine the amplitude series, the frequency L2 was used in a range of 15° to 30° in terms of the elevation angles of the satellites. Additionally, it was found that the two series had similar performances in precipitation events. Larson et al. (2008b), employed L2C modulation (6 satellites of Block IIR-M), with elevation angle range 10° to 30°, for a station located in Marshall - United States. The series of phases generated was converted empirically into a series of soil moisture. The results were validated through the series compiled from 10 in situ probes (TDR) calibrated by the gravimetric method. A correlation of 85% was obtained between these series. This research was expanded in Larson et al. (2010), with elevation angles between 5° and 25°, recorded at the NCAR station (Marshall), which is part of the active Earthscope Plate Boundary Observatory (PBO) network. The variation of the effective reflector height, or the penetration depth of waves into the ground varied according to the soil moisture content. They found that the parameter with the highest correlation with the moisture content close to the soil surface is the phase shift, which obtained a 90% correlation with FTD probes calibrated by the gravimetric method.

Rodriguez-Alvarez et al. (2009) presented the GNSS-IPT technique performed from specific equipment developed for reflectometry where the GPS hardware, in L1 frequency, was connected to a vertical linear polarization antenna. In this case, the antenna was oriented towards the horizon (Figure 4c), and the range of elevation angles between 7° e 50°. Unlike the previous cases, the SNR metric in this research was the notch, which represents the elevation angle where the minimum amplitude of the multipath oscillation occurs. The maximum soil moisture RMS error about the FDR probes was 3,1%. In later researches, Rodriguez-Alvarez et al. (2011a, and 2011b) assessed the influence of different types of land cover on GPS-IPT determinations. Arroyo et al. (2014), extended this technique to include two linear polarizations (vertical and horizontal). In this case, the SNR metrics used were the points of maximum and minimum amplitude. The correlation was 90% with a probe from the Oznet SM soil moisture monitoring network.

Chew et al. (2014) evaluated the performance of a direct model by an empirical relationship observed in field data. GPS modulations with L2 carriers were simulated, isolating and disregarding the influence of vegetation, topography, and surface roughness in modeling. The results obtained were compared with 11 FDT probes, arranged at different depths. Authors defined a gradient of soil moisture as a function of depth. By the reflectometric phase, a 91% correlation was obtained in the range between 0 and 5 centimeters depth. In Chew et al. (2015) an algorithm was developed that started to consider the effects of vegetation on modeling.

Yan et al. (2014) conducted research using a low-cost GPS receiver with frequency L1. Yan et al. (2016) used the B1 (BeiDou) and L1 (GPS) modulations with SNR obtained via NMEA 0138 sentence. Yan et al. (2017) did not directly employ SNR, but the Signal Strength Indicator, also recorded continuously by GNSS receivers.

Table 1 – Overview of related researches (published in scientific papers) related to soil moisture estimations by GNSS - R via SNR recorded in ground stations.

| Author/Year | Height (m) | Duration (days) | System | Modulation | Land Cover | Validation | Corr. (%) |
|---|---|---|---|---|---|---|---|
| Larson et al. (2008a) | 6 | 70 | G | L2 | Grass | Noah Model | - |
| Larson et al. (2008b) | 1.9 | 83 | G | L2C | Grass | TDR | 85 |

| Author/Year | Height (m) | Duration (days) | System | Modulation | Land Cover | Validation | Corr. (%) |
|---|---|---|---|---|---|---|---|
| Larson et al. (2010) | 1.8 | 210 | G | L2C | Grass | TDR | 90 |
| Rodriguez-Alvarez et al. ( 2009) | 2.6 | 60 | G | L1 | Bare | FDR | - |
| Rodriguez-Alvarez et al. (2011a) | 4.5 | 25 | G | L1 | Maize | FDR | - |
| Rodriguez-Alvarez et al. (2011b) | 3 | 600 | G | L1 | Bare | Hydra | - |
| Chew et al. (2014) | 2.4 | 230 | G | L2 | Bare | TDR | 91 |
| Arroyo et al. (2014) | 3.6 | 11 | G | L1 | Grass | OzNet SM | 90 |
| Yan et al. (2014) | 1 | 2 | G | L1 | Grass/bare | TDR | - |
| Tabibi et al. (2015) | 2 | 153 | G | L2C; L5 | Sparse veg. | TDR | 70; 80 |
| Roussel et al. (2016) | 1.7 | 40 | G; R | L1 | Bare | FDR | 95 |
| Chew et al. (2015) | 1.5to 2.1 | 730 | G | L2C | Sparse veg. | TDR | - |
| Small et al. (2016) | 2 | 730 | G | L2C | Grass | FDR | - |
| Vey et al. (2016) | 1.5 | 2100 | G | L2P; L2C | Bare | TDR | 80 |
| Yan et al. (2016) | 2 | 60 | B; G | B1; L1 | Bare | FDR | 80 |
| Yan et al. (2017) | 2 | 180 | B; G | | Bare | FDR | 70 |
| Yang et al. (2017) | 2.2 | 105 | B; G | B1, B2, L2C; L5 | Sparse veg. | Permittivity | 62;71 |
| Zhang et al. (2017) | 2.5 | 180 | G | C/A | Wheat | FDR | 74 |
| Zhang et al. (2018) | 29; 3.3 | 300; 120 | G | L2C; L5 | Grass | FDR | 86 |
| Han et al. (2018) | 1.7 | 40 | G | L1 | Soy | FDR | 95 |
| Yang et al. (2019) | 2.4 | 300 | G; B | L2C; L5; B1; B2 | Alpine veg. | TDR | 80; 85 |
| Chang et al. (2019) | 1.9 | 450 ;14 | G | L2C | Sparse veg. | Probe | 61; 87 |
| Martín et al. (2020) | 1.8 | 66 | G; R; E | L1; L1; E1 | Bare | Gravimetric | 70; 85 |
| Han et al. (2020) | 1.7 | 40 | G | L1 | Bare | FDR | 95 |

Source: The authors (2021).

In Tabibi et al. (2015), soil moisture estimations were performed using L2C and L5 signals, reaching correlations with in situ probes of 70 and 80%, respectively. Roussel et al. (2016) used GPS and GLONASS modulations recorded by a station located in Lamasquère, France, considering elevation angles between 2° and 70°.

Small et al. (2016) evaluated the performance of different algorithms aimed at removing the effects of vegetation on the reflected signals; data from 11 stations of the PBO network were used. Zhang et al. (2017) carried out simultaneous monitoring of soil moisture and vegetation growth in a wheat field in France. Yang et al. (2019) used SNR by L2C, L5, B1, and B2 obtaining correlations of up to 85%. Martín et al. (2020) used modulations by multiple constellations (GPS, GLONASS, and Galileo) by a geodetic receiver and a low-cost one. The results of this research were validated by the gravimetric method, and samples were collected daily.

## 5    DISCUSSIONS AND FINAL CONSIDERATIONS

Each of the different methods of soil moisture determination has limitations and specificities, such as the spatial scale of the measurements or footprint: sometimes punctual, as in the case of the gravimetric method and the direct in situ probes, sometimes in the order of tens of km², as in the case of remote sensing (orbital). Through these methods, there is information that may not be representative of a plot of land of interest. On the other hand, equipment such as neutron probes can provide information on an intermediate scale, however, they can be costly. In this scenario, GNSS reflectometry (GNSS-R) is an alternative or complementary method to conventional methods. Over the past decade, research has been carried out on this topic at an international level, in which results indicate a good correlation between the determinations by GNSS-R compared to conventional methods, indicating the efficiency of the technique.

GPS and GLONASS systems have global coverage and are in full operation. Currently, there are about 60 satellites considering only these two systems. Given this, there is an adequate temporal resolution for data

acquisition, due to the repetition of trajectories in terms of azimuths of passage. With the modernization of GNSS, new signals are being introduced, such as the L5, L2C, and L1C. Also, new systems such as Galileo and BeiDou have been expanding the possibilities to achieve better results in the most diverse applications in which GNSS-R can be used.

Research has also been focused on the refinement of modeling, including the evaluation of different antenna patterns (LI et al., 2018), and electromagnetic properties of the soil (WU; JIN, 2019). Investigations have evaluated the combination of techniques, especially from the CYGNSS mission, which can contribute to the spatial and temporal resolution of determinations (KIM; LAKSHMI, 2018). The CYGNSS mission has great relevance in the orbital context, as it is a constellation of eight satellites aimed at monitoring the Earth via GNSS-R (CALABIA; MOLINA; JIN, 2020).

In SNR-based GNSS-R, data from conventional GNSS stations can be used, as data from RBMC stations. Historical series of these stations can be used in reflectometry, enabling the improvement of models, calibration of satellite missions, increasing the accuracy of forecasts, and contributing to the understanding of hydrological phenomena. However, it should be noted that the use of a given sensor for this application depends on the conditions of direct visibility to the ground. In this context, many of the existing stations, mainly urban ones, do not meet this requirement.

Future research perspectives are related to investigations concerning the limitations of the technique and the improvement of modeling, highlighting the effects of the topography of the reflection surface, effects of vegetation, and roughness.

## Acknowledgments

## Author Contributions

J.F.E. carried out the initial design and writing. J.F.E., F.G.N., and C.P.K. carried out the conceptualization. All authors contributed to the review, editing, and development of the article. F.G.N. supervised the execution of the research.

## Conflicts of Interest

There are no conflicts of interest.

## References

ARORA, B.; DWIVEDI, D.; FAYBISHENKO, B.; JANA, R. B.; WAINWRIGHT, H. M. Understanding and Predicting Vadose Zone Processes. **Reviews in Mineralogy & Geochemistry,** v. 85, n. 1, p. 303-328, set. 2019. DOI.: 10.2138/rmg.2019.85.10.

ARROYO, A. A.; CAMPS, A.; AGUASCA, A.; FORTE, G. F.; MONERRIS, A.; RÜDIGER, C.; WALKER, J. P.; PACUAL, D.; ONRUBIA, R. Dual-polarization GNSS-R interference pattern technique for soil moisture mapping. **IEEE Journal of Selected Topics in Applied Earth Observations and Remote Sensing**, v. 7, n. 5, p. 1533-1544, mai. 2014. DOI.: 10.1109/JSTARS.2014.2320792.

BABAEIAN, E.; SADEGHI, M.; JONES, S. B.; MONTZKA, C.; VEREECKEN, H.; TULLER, M.. Ground, Proximal, and Satellite Remote Sensing of Soil Moisture. **Reviews of Geophysics**, v. 57, n. 2, p. 530-616, mar. 2019. DOI.: 10.1029/2018RG000618.

BILICH, A.; LARSON, K. M. Mapping the GPS multipath environment using the signal-to-noise ratio (SNR). **Radio Science**, v. 42, n. 6, nov. 2007. DOI.: 10.1029/2007RS003652.

CALABIA, A.; MOLINA, I.; JIN, S. Soil Moisture Content from GNSS reflectometry using dielectric

permittivity from fresnel reflection coefficients. **Remote Sensing**, v. 12, n. 1, p. 1-21, jan. 2020. DOI.: 10.3390/rs12010122.

CHANG, X.; JIN, T.; YU, K.; LI, Y.; LI, J.; ZHANG, Q. Soil moisture estimation by GNSS multipath signal. **Remote Sensing**, v. 11, n. 21, p. 1-16, 2019. DOI.: 10.3390/rs11212559.

CHEW, C. C.; SMALL, E. E. Soil Moisture Sensing Using Spaceborne GNSS Reflections: Comparison of CYGNSS Reflectivity to SMAP Soil Moisture. **Geophysical Research Letters**, v. 45, n. 9, p. 4049-4057, 2018. DOI.:10.1029/2018GL077905.

CHEW, C. C.; SMALL, E. E.; LARSON, K. M. An algorithm for soil moisture estimation using GPS-interferometric reflectometry for bare and vegetated soil. **GPS Solutions**, v. 20, n. 3, p. 525-537, mai. 2015. DOI.: 10.1002/2016GL068189.

CHEW, C. C.; SMALL, E. E.; LARSON, K. M.; ZAVOROTNY, V. U. Effects of near-surface soil moisture on GPS SNR data: Development of a retrieval algorithm for soil moisture. **IEEE Transactions on Geoscience and Remote Sensing**, v. 52, n. 1, p. 537-543, jan. 2014. DOI.: 10.1109/tgrs.2013.224232.

DE RIDDER, K. Surface soil moisture monitoring over Europe using Special Sensor Microwave/Imager (SSM/I) imagery. **Journal of Geophysical Research: Atmospheres**, v. 108, n. 14, 2003. DOI.: 10.1029/2002JD002796.

DESILETS, D.; ZREDA, M.; FERRÉ, T. P. A. Nature's neutron probe : Land surface hydrology at an elusive scale with cosmic rays. **Water Resources Research**, v. 46, n. 1, p. 1-7, jun. 2010. DOI.: 10.1029/2009WR008726.

DELTA-T DEVICES LTD, **User manual for the profile probe type PR1. Version PR1- UM-01-2. Delta-t Devices Ltd**, Cambridge – UK, 2001.

EDOKOSSI, K.; CALABIA, A.; JIN, S.; MOLINA, I. GNSS-reflectometry and remote sensing of soil moisture: A review of measurement techniques, methods, and applications. **Remote Sensing**, v. 12, n. 4, p. 2-26, fev. 2020. DOI.: 10.3390/rs12040614.

ENTEKHABI, D.; NJOKU, E. G.; O'NEILL, P. E.; KELLOGG, K. H.; CROW W. T.; EDELSTEIN, W N.; ENTIN, J. K.; GOODMAN, S. D.; JACKSON, T. J.; JOHNSON, J; KIMBALL, J; PIEPMEIER, J. R.; KOSTER, R. D.; NEIl, M.; MCDONALD, K. C.; MOGHADDAM, M.; MORAN, S.; REICHLE, R.; SHI, J. C.; SPENCER, M. W.; THURMAN, S. W.; TSANG, L.; VAN ZYL J. The soil moisture active passive (SMAP) mission. **Proceedings of the IEEE**, v. 98, n. 5, p. 704-716, mai. 2010. DOI.: 10.1109/JPROC.2010.2043918.

EROGLU, O.; KURUM, M.; BOYD, D.; GURBUZ, A. C. High spatio-temporal resolution CYGNSS soil moisture estimates using artificial neural networks. **Remote Sensing**, v. 11, n. 19, p. 2-32, set. 2019. DOI.: 10.3390/rs11192272.

EURIQUES, J. F. **Determinação da umidade do solo por meio da técnica de Refletometria GNSS – Primeiros resultados no Brasil**. 164 f. Dissertação (Mestrado em Ciências Geodésicas) – Programa de Pós-Graduação em Ciências Geodésicas, Universidade Federal do Paraná. Curitiba, 2019. Disponível em: https://hdl.handle.net/1884/62323. Acesso em: 20 set. 2020.

GAMARO, P. E. **Medidores Acústicos Doppler de Vazão**. 1ª ed. Foz do Iguaçu: Itaipu Binacional, 2012.

GAO, H.; WOOD, E. F.; JACKSON, T. J.; DRUSCH, M.; BINDLISH, R. Using TRMM/TMI to retrieve surface soil moisture over the southern United States from 1998 to 2002. **Journal of Hydrometeorology**, v. 7, n. 1, p. 23-38, 2006.

GEORGIADOU, P. Y.; KLEUSBERG, A. On Carrier Signal Multipath Effects in Relative GPS Positioning. **Manuscripta Geodaetica**, v. 13, n. 1, p. 172-179, 1988.

GLEASON, S.; HODGART, S.; SUN, Y.; GOMMENGINGER, C.; MACKIN, S.; ADJRAD, UNWIN, M. Detection and Processing of Bistatically reflected GPS signals from Low Earth Orbit for the purpose of Ocean Remote Sensing. **IEEE Transactions on Geoscience and Remote Sensing**, v. 43, n. 6, p. 1229-1241, jul. 2005. DOI.: 10.1109/TGRS.2005.845643.

GURTNER, W.; ESTEY, L. **RINEX The Receiver Independent Exchange Format Version 3.03**. 2015. Astronomical Institute, University of Bern and UNAVCO. Disponível em: < ftp://igs.org/pub/data/format/rinex300.pdf > Acesso em 23 set. 2020.

HALLIKAINEN M.T.; F.T. ULABY; M.C. DOBSON; M. EL-RAYES; WU, L.-K. Microwave Dielectric Behaviour of Wet Soil - Part 1: Empirical Models and Experimental Observations. **IEEE Transactions on Geoscience and Remote Sensing**, v. 23, n. 1, p. 25-34, jan. 1985. DOI.: 10.1109/TGRS.1985.289497.

HAN, M.; ZHU, Y.; YANG, D.; CHANG, Q.; HONG, X.; SONG, S. Soil moisture monitoring using GNSS interference signal: proposing a signal reconstruction method. **Remote Sensing Letters**, v. 11, n. 4, p. 373-382, 2020. DOI.: 10.1080/2150704X.2020.1718235.

HAN, M.; ZHU, Y.; YANG, D.; HONG, X.; SONG, S. A semi-empirical SNR model for soil moisture retrieval using GNSS SNR data. **Remote Sensing**, v. 10, n. 2, p. 1-19, 2018. DOI.:10.3390/rs10020280.

HANSON, B. Field Estimation of Soil Water Content: A Practical Guide to Methods, Instrumentation and Sensor Technology. **Vadose Zone Journal**, v. 8, n. 3, p. 628-759, 2009. DOI.: 10.2136/vzj2008.0171.

HILLEL, D. **Environmental Soil Physics**. 1º ed. San Diego: Academic Press, 1998.

JIA, Y.; PEI, Y. Remote Sensing in Land Applications by Using GNSS-Reflectometry. In: HUNG, M.; WU, Y. **Recent Advances and Applications in Remote Sensing**. IntechOpen, 2018. p. 65-88.

JIN, S.; CARDELLACH, E.; XIE, F. **Remote Sensing and Digital Image Processing: Theory, Methods and Applications**. 2014. Dordrecht: Springer, 2014.

JIN, S.; QIAN, X.; KUTOGLU, H. Snow depth variations estimated from GPS-reflectometry: A case study in Alaska from L2P SNR data. **Remote Sensing**, v. 8, n. 1, p. 1-15 jan. 2016. DOI: 10.3390/rs8010063.

KATZBERG, S. J.; TORRES, O.; GRANT, M. S.; MASTERS, D. Utilizing calibrated GPS reflected signals to estimate soil reflectivity and dielectric constant: Results from SMEX02. **Remote Sensing of Environment**, v. 100, n. 1, p. 17-28, set. 2006. DOI.: 10.1016/j.rse.2005.09.015.

KERR, Y. H.; WALDTEUFEL, P.; WIGNERON, J. P.; MARTINUZZI, J. M.; FONT, J.; BERGER, M. Soil Moisture Retrieval from Space: The Soil Moisture and Ocean Salinity (SMOS) Mission. **IEEE Transactions on Geoscience and Remote Sensing,** v. 39, n. 8, p. 1729-1735, 2001. DOI.: 10.1109/36.942551.

KIM, H.; LAKSHMI, V. Use of Cyclone Global Navigation Satellite System (CYGNSS) Observations for Estimation of Soil Moisture. **Geophysical Research Letters**, v. 45, n. 16, p. 8272–8282, 2018. DOI.: 10.1029/2018GL078923.

LARSON, K. M. GPS interferometric reflectometry: applications to surface soil moisture, snow depth, and vegetation water content in the western United States. **Wiley Interdisciplinary Reviews: Water,** v. 3, n. 6, p. 775-787, 2016. DOI.:10.1002/wat2.1167.

LARSON, K. M.; BRAUN, J. J.; SMALL, E. E.; ; ZAVOROTNY, V. U.; GUTMANN, E. D.; BILICH A. L. GPS Multipath and Its Relation to Near-Surface Soil Moisture Content. **IEEE Journal of Selected Topics in Applied Earth Observations and Remote Sensing**, v. 3, n. 1, p. 91-99, 2010. DOI.: 10.1109/jstars.2009.2033612.

LARSON, K. M.; NIEVINSKI, F. G. GPS snow sensing: results from the EarthScope Plate Boundary Observatory. **GPS Solutions**, v. 17, n. 1, p. 41-52, 2013. DOI.: 10.1007/s10291-012-0259-7.

LARSON, K. M.; SMALL, E. E.; GUTMANN, E.; BILICH, A. L.; AXELRAD, P.; BRAUN, J. Using GPS multipath to measure soil moisture fluctuations: Initial results. **GPS Solutions**, v. 12, n. 3, p. 173-177, 2008a. DOI.: 10.1007/s10291-007-0076-6.

LARSON, K. M.; SMALL, E. E.; GUTMANN, E. D; BILICH, A. L.; BRAUN, J. J.; ZAVOROTNY V. U. Use of GPS receivers as a soil moisture network for water cycle studies. **Geophysical Research Letters**, v. 35, n. 24, dez. 2008b. p. 1-5. DOI.:10.1029/2008gl036013.

LEICK, A. **GPS Satellite Surveying**. 2ª ed. New York: John Wiley & Sons, 1995.

LI, F.; PENG, X.; CHEN, X.; LIU, M.; XU, L. Analysis of key issues on GNSS-R soil moisture retrieval based on different antenna patterns. **Sensors,** v. 18, n. 8, p. 1-16, ago. 2018. DOI.: 10.3390/s18082498.

LIU, L.; LARSON, M. Decadal changes of surface elevation over permafrost area estimated using reflected GPS signals. **Cryosphere**, v. 12, n. 2, p. 477-489, fev. 2018. DOI.: 10.5194/tc-12-477-2018.

LIMA, J.; SILVA, E.; KOIDE, S.; SANTOS, R. Avaliação do Desempenho de Sonda de Capacitância no Monitoramento da Umidade de Latossolos do Cerrado em Condições de Campo. **Revista Brasileira de Recursos Hídricos**, v. 17, n. 1, p. 23-32, nov. 2012. DOI.:10.21168/rbrh.v17n1.p23-32.

LÖFGREN, J. S.; HAAS, R. Sea level measurements using multi-frequency GPS and GLONASS observations. **Eurasip Journal on Advances in Signal Processing**, v. 2014, n. 1, 2014. DOI: 10.1186/1687-6180-2014-50.

MARTIN-NEIRA, M. A Passive Reflectometry and Interferometry System (PARIS): application to ocean altimetry. **European Space Agency Journal**, v. 17, p. 331-355, 1993.

MARTÍN, A.; IBÁÑEZ, S.; BAIXAULI, C., BLANC, S.; ANQUELA, A. B. Multi-constellation GNSS interferometric reflectometry with mass-market sensors as a solution for soil moisture monitoring. **Hydrology and Earth System Sciences**, v. 24, p. 3573-3582, jul. 2020. DOI.: 10.5194/hess-24-3573-2020.

MASTERS, D.; AXELRAD, P.; KATZBERG, S. Initial results of land-reflected GPS bistatic radar measurements in SMEX02. **Remote Sensing of Environement**, v. 92, p. 507-520, mai. 2004. DOI.: 10.1016/j.rse.2004.05.016.

MENDES, P. C. de S. **Caracterização de um sensor para medição de umidade do solo com termo-resistor a temperatura constante**. 127 f. Tese (Doutorado em Engenharia Elétrica) – Programa de Pós-Graduação em Engenharia Elétrica, Universidade Federal da Bahia, Salvador, 2006.

MONICO, J. F. G. **Posicionamento pelo GNSS: Descrição, Fundamentos e Aplicações**. 2ª ed. Presidente Prudente: Editora Unesp, 2008.

NIEVINSKI, F. G.; LARSON, K. M. Forward modeling of GPS multipath for near-surface reflectometry and positioning applications. **GPS Solutions,** v. 18, n. 2, p. 309-322, 2014a. DOI.:10.1007/s10291-013-0331-y.

NIEVINSKI, F. G.; LARSON, K. M. An open source GPS multipath simulator in Matlab/Octave. **GPS Solutions**, v. 18, n. 3, p. 473-481, Fev. 2014b. DOI.:10.1109/tgrs.2013.2297688.

NIEVINSKI, F. G.; LARSON, K. M. Inverse modeling of GPS multipath for snow depth estimation - Part I: Formulation and simulations. **IEEE Transactions on Geoscience and Remote Sensing**, v. 52, n. 10, p. 6555-6563, 2014c. DOI.:10.1109/TGRS.2013.2297681.

NIEVINSKI, F. G.; LARSON, K. M. Inverse modeling of GPS multipath for snow depth estimation - Part II: Application and validation. **IEEE Transactions on Geoscience and Remote Sensing**, v. 52, n. 10, p. 6564–6573, 2014d. DOI.:10.1109/tgrs.2013.2297688.

NIEVINSKI, F. G., MONICO, J. F. G. GPS como um sensor remoto. In: PARANHOS FILHO, A. C.; MIOTO, C. L.; MARCATO JUNIOR, J.; CATALANI, T. G. T. (Org.). **Geotecnologias em Aplicações Ambientais**. 1ª ed. Campo Grande: Editora da UFMS, 2016, vol.1, p.234-251.

NIEVINSKI, F. G.; SILVA, M. F. E.; BONIFACE, K.; MONICO, J. F. G. GPS Diffractive Reflectometry: Footprint of a Coherent Radio Reflection Inferred from the Sensitivity Kernel of Multipath SNR. **IEEE Journal of Selected Topics in Applied Earth Observations and Remote Sensing**, v. 9, n. 10, p. 4884-4891, Out. 2016. DOI.:10.1109/jstars.2016.2579599.

OCHSNER, T. E.; COSH, M. H.; CUENCA, R. H.; DORIGO,W.A.; DRAPER, C.S.; HAGIMOTO,Y.; KERR, Y.; LARSON, K.M.; NJOKU, E. G.; SMALL, E. R.; ZREDA, M. State of the Art in Large-Scale Soil Moisture Monitoring. **Soil Science Society of America Journal**, v. 77, n. 6, p. 1888-1923, 2013. DOI.:10.2136/sssaj2013.03.0093.

PEREIRA, S. **Tecnologia da Reflectometria no Domínio do Tempo para medição da umidade do solo**.

109 f. Tese (Doutorado em Engenharia Agrícola) – Programa de Pós-Graduação em Engenharia Agrícola, Universidade Federal de Viçosa, Viçosa, 2011.

ROBINSON, D. A.; CAMPBELL, C. S.; HOPMANS, J. W.; HORNBUCKLE, B. K.; JONES, S. B.; KNIGHT, R.; OGDEN, F.; SELKER, J.; WENDROTH, O. Soil Moisture Measurement for Ecological and Hydrological Watershed-Scale Observatories: A Review. **Vadose Zone Journal**, v. 7, n. 1, p. 358-389, fev. 2008. DOI.: 10.2136/vzj2007.0143.

RODRIGUEZ-ALVAREZ, N.; AKOS, D. M.; ZAVOROTNY, V. U.; SMITH, J. A.; CAMPS, A.; FAIRALL, C. W. Airborne GNSS-R Wind Retrievals Using Delay – Doppler Maps. **IEEE Transactions on Geoscience and Remote Sensing**, v. 51, n. 1, p. 626-641, jan. 2013. DOI.: 10.1109/TGRS.2012.2196437.

RODRIGUEZ-ALVAREZ, N.; BOSCH-LLUIS, X.; CAMPS, A.; VALL-LLOSSERA, M.; VALENCIA, E.; MARCHAN-HERNANDEZ, J. F.; RAMOS-PEREZ, I.. Soil moisture retrieval using GNSS-R techniques: Experimental results over a bare soil field. **IEEE Transactions on Geoscience and Remote Sensing**, v. 47, n. 11, p. 3616-3624, 2009. DOI.: 10.1109/TGRS.2009.2030672.

RODRIGUEZ-ALVAREZ, N.; CAMPS, A.; VALL-LLOSSERA, M.; M.; BOSCH-LLUIS, X.; MONERRIS, A.; RAMOS-PEREZ, I.; VALENCIA, E.; MARCHAN-HERNANDEZ, F.; MARTINEZ-FERNANDEZ, J.; BARONCINI-TURRICCHIA, G.; PÉREZ-GUTIÉRREZ, C.; SÁNCHEZ, N. Land geophysical parameters retrieval using the interference pattern GNSS-R technique. **IEEE Transactions on Geoscience and Remote Sensing**, v. 49, n. 1, p.71-84, Jan. 2011a. DOI.:10.1109/TGRS.2010.2049023.

RODRIGUEZ-ALVAREZ, N.; BOSCH-LLUIS, X.; CAMPS, A.; AGUASCA, A.; VALL-LLOSSERA, M.; VALENCIA, E.; RAMOS-PEREZ, I.; PARK, H. Review of crop growth and soil moisture monitoring from a ground-based instrument implementing the Interference Pattern GNSS-R Technique. **Radio Science**, v. 46, n. 5, p. 1-11, out. 2011b. DOI.: 10.1029/2011RS004680.

ROUSSEL, N.; FRAPPART, F.; RAMILLIEN, G.; DARROZES, J.; BAUP, F.; LESTARQUIT, L.; HA, M. C. Detection of Soil Moisture Variations Using GPS and GLONASS SNR Data for Elevation Angles Ranging from 2° to 70°. **IEEE Journal of Selected Topics in Applied Earth Observations and Remote Sensing**, v. 9, n. 10, p. 4781-4794, 2016. DOI.:10.1109/JSTARS.2016.2537847.

SEEBER, G. **Satellite Geodesy: Foundations, Methods, and Applications**. 2ª ed. New York: Walter de Gruyter, 2003.

SENEVIRATNE, S. I.; CORTI, T.; DAVIN, E. L.; HIRSCHI, M.; JAEGER, E. R.; LEHNER, I. ORLOWSKY, B.; TEULING, A. J. Investigating soil moisture-climate interactions in a changing climate: A review. **Earth-Science Reviews**, v. 99, n. 4, p. 125-161, fev. 2010. DOI.:10.1016/j.earscirev.2010.02.004.

SMALL, E. E.; LARSON, K. M.; CHEW, C. C.; DONG, J.; OCHSNER, T. E. Validation of GPS-IR Soil Moisture Retrievals: Comparison of Different Algorithms to Remove Vegetation Effects. **IEEE Journal of Selected Topics in Applied Earth Observations and Remote Sensing**, v. 9, n. 10, p. 4759-4770, out. 2016. DOI.: 10.1109/JSTARS.2015.2504527.

STRANDBERG, J.; HOBIGER, T.; HAAS, R. Coastal Sea Ice Detection Using Ground-Based GNSS-R. **IEEE Geoscience and Remote Sensing Letters**, v. 14, n. 9, p. 1552–1556, 2017. DOI.: 10.1109/LGRS.2017.2722041.

SWENSON, S.; FAMIGLIETTI, J.; BASARA, J.; WAHR, J. Estimating profile soil moisture and groundwater variations using GRACE and Oklahoma Mesonet soil moisture data. **Water Resources Research**, v. 44, n. 1, p. 1-12, 2008. DOI.:10.1029/2007WR006057.

TABIBI, S.; NIEVINSKI, F. G.; VAN DAM, T. Statistical Comparison and Combination of GPS, GLONASS, and Multi-GNSS Multipath Reflectometry Applied to Snow Depth Retrieval. **IEEE Transactions on Geoscience and Remote Sensing**, v. 55, n. 7, p. 3773-3785, 2017. DOI.:10.1109/tgrs.2017.2679899.

TABIBI, S.; NIEVINSKI, F. G.; VAN DAM, T.; MONICO, J. F. G. Assessment of modernized GPS L5 SNR for ground-based multipath reflectometry applications. **Advances in Space Research**, v. 55, n. 4, p. 1104-1116, 2015. DOI.:10.1016/j.asr.2014.11.019.

TEUNISSEN, P. J.; MONTENBRUCK, O. **Springer Handbook of Global Navigation Satellite Systems**. [s.l.]: Springer International Publishing, 2017. DOI 10.1007/978-3-319-42928-1

TULLER, M.; OR, D. Water Retention and Characteristic Curve. In: HILLEL, D; HATFIELD, J. L.; POWLSON, D. S.; ROSENZWEIG, C..; SCOW, K. M.; SINGER, J. M.; SPARKS, D. L. **Encyclopedia of Soils in the Environment**, 1º ed., Amsterdã, Elsevier Academic Press, 2004, p. 278-289. ISBN**:** 9780123485304.

VEY, S.; GÜNTNER, A.; WICKERT, J.; BLUME, T.; RAMATSCHI, M. Long-term soil moisture dynamics derived from GNSS interferometric reflectometry: a case study for Sutherland, South Africa. **GPS Solutions**, v. 20, n. 4, p. 641-654, 2016. DOI.: 10.1007/s10291-015-0474-0.

WU, X.; JIN, S. A Simulation Study of GNSS-R Polarimetric Scattering from the Bare Soil Surface Based on the AIEM. **Advances in Meteorology**, v. 2019, p. 1-9, mai. 2019. DOI.: 10.1155/2019/3647473.

XIE, Q.; MENENTI, M.; JIA, L. Improving the AMSR-E/NASA soil moisture data product using in-situ measurements from the Tibetan Plateau. **Remote Sensing,** v. 11, n. 23, 2019. DOI.:10.3390/rs11232748.

YAN, S.; LI, Z.; YU, K.; ZHANG, K. GPS-R L1 interference signal processing for soil moisture estimation: an experimental study. **Eurasip Journal on Advances in Signal Processing**, v. 107, n. 1, p. 1-13, 2014. DOI.: 10.1186/1687-6180-2014-107.

YAN, S. H.; ZHANG, N.; CHEN, N. C.; GONG, J. Y. Feasibility of using signal strength indicator data to estimate soil moisture based on GNSS interference signal analysis. **Remote Sensing Letters**, v. 9, n. 1, p. 61-70, 2017. DOI.:10.1080/2150704X.2017.1384587.

YAN, S. H.; ZHAO, F.; CHEN, N. C.; GONG, J. Y. Soil moisture estimation based on BeiDou B1 interference signal analysis. **Science China Earth Sciences**, v. 59, n. 12, p. 2427-2440, 2016. DOI.: 10.1007/s11430-015-0013-7.

YANG, T.; WAN, W.; CHEN, X.; CHU, T.; QIAO, Z.; LIANG, H.; WEI. J.; WANG, G.; HONG, Y. Land surface characterization using BeiDou signal-to-noise ratio observations. **GPS Solutions**, v. 23, n. 2, p. 1–12, 2019. DOI .10.1007/s10291-019-0824-4.

YANG, T.; WAN, W.; CHEN, X.; CHU, T.; HONG, Y. Using BDS SNR observations to measure near-surface soil moisture fluctuations: Results from low vegetated surface. **IEEE Geoscience and Remote Sensing Letters**, v. 14, n. 8, p. 1308-1312, 2017. DOI.: 10.1109/LGRS.2017.2710083.

ZAVOROTNY, V. U.; LARSON, K. M.; BRAUN, J. J.; SMALL, E. E.; GUTMANN, E. D.; BILICH, A. L. A Physical Model for GPS Multipath Caused by Land Reflections : Toward Bare Soil Moisture Retrievals. **IEEE Journal of Selected Topics in Applied Earth Observations and Remote Sensing**, v. 3, n.1, p. 100-110, 2010, abr. 2010. DOI.: 10.1109/JSTARS.2009.203360.

ZAVOROTNY, V. U.; GLEASON, S.; CARDELLACH, E.; CAMPS, A. Tutorial on remote sensing using GNSS bistatic radar of opportunity. **IEEE Geoscience and Remote Sensing Magazine**, v. 2, n. 4, p. 8-45, 2015. DOI.:10.1109/MGRS.2014.2374220.

ZHANG, S.; ROUSSEL, N.; BONIFACE, K.; HA, C. M.; FRAPPART, F.; DARROZES, J.; BAUP, F.; CALVET, J. C. Use of reflected GNSS SNR data to retrieve either soil moisture or vegetation height from a wheat crop. **Hydrology and Earth System Sciences**, v. 21, n. 9, p. 4767-4784, 2017. DOI.:10.5194/hess-21-4767-2017.

ZHANG, S.; CALVET, J. C.; DARROZES, J.; ROUSSEL, N.; FRAPPART, F.; BOUHOURS, G. Deriving surface soil moisture from reflected GNSS signal observations from a grassland site in southwestern France. **Hydrology and Earth System Sciences**, v. 22, n. 3, p. 1931-1946, 2018. DOI.: 10.5194/hess-22-1931-2018.

ZHANG, F.; ZHANG, L.-W.; SHI, J.-J.; HUANG, J.-F. Soil Moisture Monitoring Based on Land Surface Temperature-Vegetation Index Space Derived from MODIS Data. **Pedosphere**, v. 24, n. 4, p. 450-460, 2014. DOI.: 10.1016/S1002-0160(14)60031-X.

ZHOU, W.; LIU, L.; HUANG, L.; YAO, Y.; CHEN, J.; LI, S. A New GPS SNR-based Combination Approach

for Land Surface Snow Depth Monitoring. **Scientific Reports**, v. 9, n. 1, p. 1-20, mar. 2019. DOI.: 10.1038/s41598-019-40456-2.

ZREDA, M.; SHUTTLEWORTH, W. J.; ZENG, X.; DESILETS, D.; FRANZ, T.; ROSOLEM, R. COSMOS: The cosmic-ray soil moisture observing system. **Hydrology and Earth System Sciences**, v. 16, n. 11, p. 4079-4099, 2012. DOI.:10.5194/hess-16-4079-2012.

## First Author bigraphy

Jorge Felipe Euriques is a Cartographer and Surveyor engineer who graduated from the Federal University of Paraná (UFPR). He has international experience through an academic mobility at the École Supérieure des Géométres et Topographes – France. He received a master's degree in Geodetic Sciences in 2019 from UFPR. He is a member of the Space Geodesy and Hydrography Laboratory at the Department of Geomatics - UFPR since 2014. He worked at the Cadastral and Geoprocessing Service of the municipal government of São Bento do Sul (SC) (2004-2010). He is currently a Ph.D. student in the Graduate Program in Geodetic Sciences. His main research interests include GNSS positioning, GNSS Reflectometry, and GNSS antenna calibrations.